

Dynamics of Laser Eigenstates

A. Le Floch, G. Ropars, and J. M. Lenormand

Laboratoire d'Electronique Quantique, Université de Rennes, F-35042 Rennes Cédex, France

and

R. Le Naour

Laboratoire d'Electronique Quantique, Université de Nantes, F-44072 Nantes Cédex, France

(Received 22 August 1983)

The spatial representation of the generalized potentials associated with the two eigenstates of a quasi-isotropic laser, in the frame of the Landau theory, predicts two different types of first-order phase transitions. The different dynamics of the corresponding vectorial bistabilities are confirmed by an experiment with a laser with two oscillating nondegenerate eigenstates. Polarization instabilities predicted in the first type of transition are experimentally shown.

PACS numbers: 42.55.Bi, 42.60.He

Great interest has been shown in recent years in bistability¹⁻³ and instabilities⁴⁻⁷ of nonlinear optical systems. Most of the devices, especially the intrinsic ones, are concerned with scalar bistability, the intensity being the essential parameter. However, vectorial bistability was observed in the earlier years of laser physics, exhibiting some hysteresis phenomena.⁸ Unfortunately the dynamics of this bistability were of great complexity from both the experimental^{8,9} and the theoretical^{10,11} points of view. Indeed the experiments need quasi-isotropic lasers, so as to allow the oscillation of the two nearly degenerate eigenstates, which are defined by the resonance condition¹² $M\vec{E} = \lambda\vec{E}$. The 2×2 Jones matrix M represents a complete round-trip pass in the cavity, each optical element being represented by its own Jones matrix. We propose in this Letter to extend the Landau theory of phase transitions to describe the spatial evolution of the two eigenstates of a laser. Although the system is not in thermal equilibrium,¹³ this model with two spatially competing order parameters¹⁴ provides new insights into eigenstate dynamics and allows us to predict two mechanisms corresponding to two different first-order phase transitions. These predictions are experimentally confirmed and may lead to vectorial instabilities and intrinsic fast switches with low-level background. The phase-transition model has already been used to describe injected-external-signal lasers,^{15,16} lasers with saturable absorbers,¹⁷ and macroscopic quantum fluctuations in a laser.¹⁸

Let us call \vec{E}_x and \vec{E}_y the two eigenstates oscillating in a laser with an adjustable linear phase anisotropy $\Delta\phi_{xy}$. The eigenstate degeneracy is then removed with respect to the polarization and to the

frequency. The equations of evolution of the eigenstates may be written in a form derived from the Lamb theory¹⁹:

$$\begin{aligned}\dot{E}_x &= E_x(\alpha_x - \beta_x E_x^2 - \theta_{xy} E_y^2) + q_x(t), \\ \dot{E}_y &= E_y(\alpha_y - \beta_y E_y^2 - \theta_{xy} E_x^2) + q_y(t),\end{aligned}\quad (1)$$

where α_x and α_y include losses and characterize the "net gain" of the two eigenstates, β_x and β_y their self-saturations, and θ_{xy} their coupling. The Langevin noise terms, $q_x(t)$ and $q_y(t)$, represent the spontaneous-emission fluctuations. The steady-state solution for the amplitude of the two competing eigenstates can be associated, as in an injected-external-signal laser,¹⁵ with a potential

$$\begin{aligned}V(E_x, E_y) &= -\frac{1}{2}\alpha_x E_x^2 - \frac{1}{2}\alpha_y E_y^2 + \frac{1}{4}\beta_x E_x^4 \\ &\quad + \frac{1}{4}\beta_y E_y^4 + \frac{1}{2}\theta_{xy} E_x^2 E_y^2.\end{aligned}$$

Such a potential allows us to represent the whole system with the spatial diagram of Fig. 1(a). On the x and y axes this potential reduces to $V(E) = -\frac{1}{2}\alpha E^2 + \frac{1}{4}\beta E^4$ as for the usual laser with a single oscillating eigenstate. When the degeneracy of the eigenstate frequencies is removed by an intracavity birefringence, the tuning of the laser frequency across the gain curve [Fig. 1(b)] allows us to vary the relative heights of the working points A and B . An investigation of the eigenstate dynamics versus the frequency dependence is then possible. This simple spatial diagram suggests two possibilities for the eigenstate dynamics. The system may move from A to B using two paths: (i) *The electric field rotates in the transverse plane*, the system going along the AMB line with a frequency drift. (ii) *A mode in-*

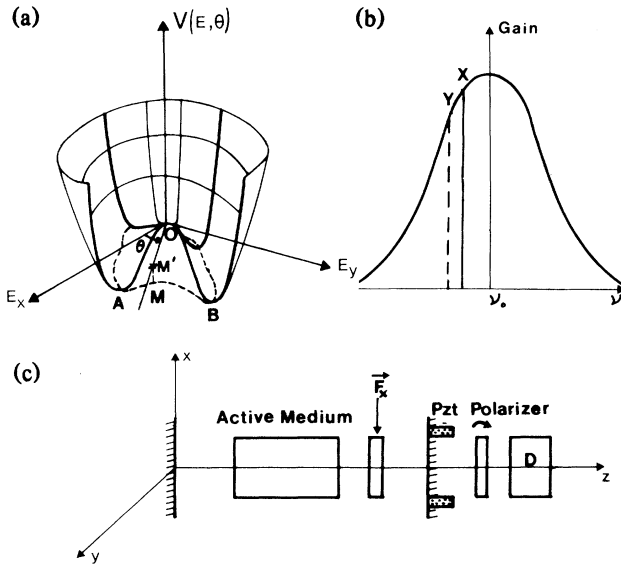


FIG. 1. (a) Spatial representation of the generalized potentials. (b) Positions of x and y eigenstates for $\vec{F}_x \neq 0$. (c) Experimental setup.

hibition takes place along the AOB path. A discussion of the stability of the two eigenstates in the two processes predicted by the spatial diagram may be done as for the usual two-mode laser with the two modes oscillating on the same eigenstate.¹⁹ Suppose that the laser oscillates around \vec{E}_x . If ϵ_y is the small component on the y axis, the equation of motion for ϵ_y is written as

$$\dot{\epsilon}_y = \epsilon_y (\alpha_y - \theta_{xy} \alpha_x / \beta_x) + O(\epsilon^3), \quad (2)$$

where the $O(\epsilon^3)$ term is negligible and $\alpha_x / \beta_x = E_x^2$. The eigenstate flips occur when the sign of the expression in parentheses changes and becomes positive. In both processes the intensity remains quasiconstant during the flips, when there is no other anisotropic loss in the cavity.

First, the rotation process requires a supplementary relation between the x and y eigenstates, i.e., $E_x = E_0 \cos \theta$ and $E_y = E_0 \sin \theta$, where θ describes the vector rotation in the x - y plane. In this process where E_x and E_y have the same frequency, the potential representing the whole system may be written as a single oscillating eigenstate. The spatial variation $\Delta V(E_0, \theta)$ is readily obtained by noting that, when θ varies, the x and y components of the electric field cannot simultaneously be at cavity resonance in a nondegenerate-eigenstate laser, resulting in related losses. Indeed the loss term $\Delta p(\theta)$ may be calculated for each value of the phase anisotropy $\Delta \phi_{xy}$ as a function of the cavity finesse F ,

i.e.,

$$\Delta p(\theta) = F^2 \sin 2\theta (\sin \theta + \cos \theta) \Delta \phi_{xy}^2 / 2\pi^2. \quad (3)$$

If this loss term is introduced into the $\alpha(\theta)$ coefficient of the potential, we obtain the variation $\Delta V(E_0, \theta)$ describing the AMB barrier. The minima occur for $\theta = 0^\circ$ and 90° . For the maximum defined at $\theta = \pi/4$ the Δp value is $\Delta p(\pi/4) = F^2 \Delta \phi_{xy}^2 / \sqrt{2} \pi^2$. Furthermore, if $\Delta \phi_{xy} \approx 0$, the loss vanishes and the potential $V(E_0, \theta)$ becomes flat with respect to its θ dependence, leading to the possibility of vectorial instabilities for the eigenstate rotation dynamics as predicted by the Landau theory.²⁰ This two-valley potential curve implies the existence of a first-order transition, i.e., of a hysteresis loop. Moreover, we note that, at a given eigenstate flip frequency, an increase of the barrier AMB due to an increase of the value of $\Delta \phi_{xy}$ forbids the flip. Indeed, within the parentheses in Eq. (2), α_y decreases with an increase of the losses associated with the y component, which is then not tuned to the cavity. So the expression in parentheses remains negative. To restore the flip one needs to scan the system to a higher slope on the gain curve of Fig. 1(b), introducing a greater difference of heights between the potentials at A and B and thereby increasing the hysteresis loop.

On the other hand, when the barrier AMB becomes too high, the rotation mechanism no longer occurs, but the path AOB becomes possible if the AOB barrier is lowered. In this inhibition mechanism the x eigenstate intensity decreases and the y eigenstate intensity increases at a slightly different frequency, with $E_x^2(\nu_x) + E_y^2(\nu_y) = E_0^2$. Here, each eigenstate remains at cavity resonance and equal losses occur in α_x and α_y . The sign change of the expression in parentheses in Eq. (2) may in this case be obtained by a reduction of the nonlinear negative term either by tuning the laser towards the threshold frequency to reduce $I_x = \alpha_x / \beta_x$ or by increasing $\Delta \phi_{xy}$ to reduce θ_{xy} . The physical meaning is the reduction of the barrier AOB , allowing the second mechanism to work. A further increase in $\Delta \phi_{xy}$ reduces the atomic coupling coefficient θ_{xy} even more, changing the sign of the expression in parentheses in Eq. (2), i.e., reducing the hysteresis loop. So the two expected processes of different nature both lead to first-order phase transitions. However, their properties will be quite different with respect to the phase anisotropy variations, the photon statistics,²¹ and the possibility of vectorial instabilities.

The experimental evidence of the two mechanisms and of their main properties is obtained with a

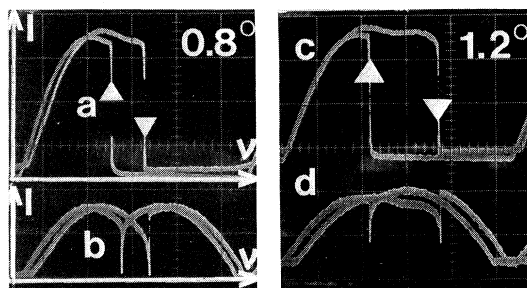


FIG. 2. The rotation mechanism. (a) Output power I of the x eigenstate polarization vs frequency for $\Delta\phi_{xy} = 0.8^\circ$ (I axis, $3 \mu\text{W}/\text{div}$; ν axis, $60 \text{ MHz}/\text{div}$). (b) I with polarizer rotated at $\theta = \pi/4$ for $\Delta\phi_{xy} = 0.8^\circ$. (c) Same as (a) for $\Delta\phi_{xy} = 1.2^\circ$. Same as (b) for $\Delta\phi_{xy} = 1.2^\circ$.

$3.39\text{-}\mu\text{m } ^3\text{He-}^{20}\text{Ne}$ laser as shown in Fig. 1(c). The magnetically shielded cell ends with quasiperpendicular windows, and an additional stressed window gives the main and adjustable linear phase anisotropy which may be measured outside the cavity. The force \vec{F}_x leads to a longer optical path along the y axis than along the x axis. Therefore, on the low-frequency side, the oscillation begins on the x eigenstate [Fig. 1(b)]. A polarizer allows us to investigate the frequency hysteresis domain, and also to detect a rotation mechanism when it is rotated to $\pm 45^\circ$ from the x axis. Indeed this mechanism gives an extinction (dip) or a doubling (peak) of the transmitted intensity during the eigenstate flips. With $\Delta\phi_{xy} \approx 0.8^\circ$, which corresponds to a relatively weak barrier $\Delta V(E_0, \theta)$, the hysteresis domain is shown in Fig. 2(a). The dips in Fig. 2(b) prove the existence of the rotation mechanism. A greater value, $\Delta\phi_{xy} \approx 1.2^\circ$, gives, as predicted for the first mechanism, a *greater hysteresis domain* [Fig. 2(c)]. When the $\Delta\phi_{xy}$ value reaches about 1.5° which corresponds to a loss $\Delta p(\pi/4) \approx 0.5\%$, the first mechanism stops. The dips in Figs. 2(b) and 2(d) abruptly disappear. The x eigenstate oscillates until the second mechanism appears for a sufficiently low intensity near the threshold. The hysteresis domain occurs indeed over almost the whole laser profile, as shown in Fig. 3(a). In this inhibition mechanism, the *hysteresis loop shrinks*, as shown in Figs. 3(c) and 3(e), for further increased values of $\Delta\phi_{xy}$, in agreement with the predictions. The $\pm 45^\circ$ polarizer test shows neither dips nor peaks, as shown in Figs. 3(d) and 3(f), excluding therefore the rotation mechanism. The two types of first-order transitions corresponding to the two paths are clearly identified. Moreover, note that by reducing the excitation, with the rotational losses remaining constant,

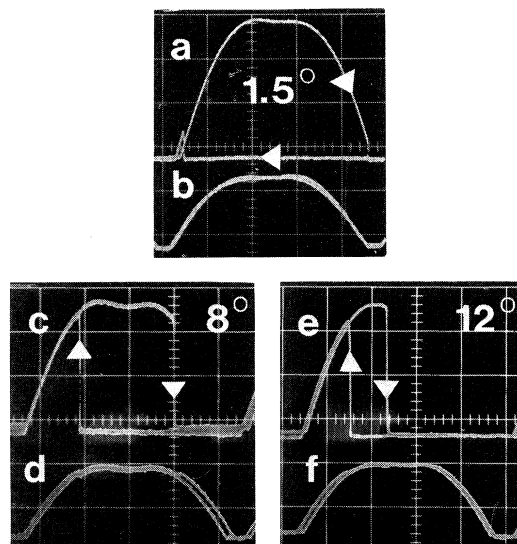


FIG. 3. The inhibition mechanism. (a) Same as in Fig. 2(a) for $\Delta\phi_{xy} = 1.5^\circ$. (b) Same as in Fig. 2(b) for $\Delta\phi_{xy} = 1.5^\circ$. (c) Same as (a) for $\Delta\phi_{xy} = 8^\circ$. (d) Same as (b) for $\Delta\phi_{xy} = 8^\circ$. (e) Same as (a) for $\Delta\phi_{xy} = 12^\circ$. (f) Same as (b) for $\Delta\phi_{xy} = 12^\circ$.

it is always possible to reduce the barrier AOB compared to the barrier AMB . This is confirmed by the experiment; the rotational peaks that exist for $\Delta\phi_{xy} = 0.8^\circ$ for instance abruptly disappear when the excitation is decreased and the inhibition process appears. Furthermore, the possibility of observing vectorial instabilities is easily obtained when $\Delta\phi_{xy}$ goes to zero, the rotational first-order transition potential being flattened in its θ dependence. This is shown in Fig. 4(b) for the whole oscillation domain. If the frequency tuning of the laser is stopped, the instabilities remain and are observed versus time with a $7\text{-}\mu\text{s}$ period, as in Fig. 4(c).

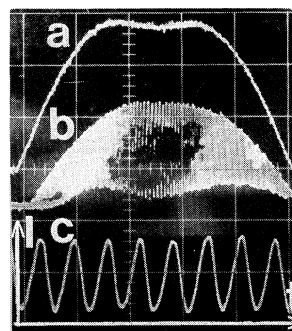


FIG. 4. Vectorial instabilities for $\Delta\phi_{xy} \approx 0^\circ$. Output power (a) vs frequency without polarizer, (b) vs frequency with polarizer, and (c) vs time at fixed frequency ($10 \mu\text{s}/\text{div}$).

In conclusion, the spatial extension of the Landau theory, in the study of the dynamics of laser eigenstates, predicts two different types of first-order phase transitions which are experimentally confirmed. These dynamics may lead to new intrinsic devices based on the vectorial bistabilities and instabilities and may give new insights in two-eigenstate-laser injection locking experiments. Similar eigenstate dynamics are expected on other types of lasers with different basic eigenstates.

This work was supported by the Centre National de la Recherche Scientifique and the Direction des Recherches, Etudes, et Techniques.

-
- ¹H. M. Gibbs *et al.*, Phys. Rev. Lett. 36, 1135 (1976).
²V. P. Chebotayev *et al.*, IEEE J. Quantum Electron. 4, 788 (1968).
³P. W. Smith and E. H. Turner, Appl. Phys. Lett. 30, 280 (1977).
⁴S. L. McCall, Appl. Phys. Lett. 32, 284 (1978).
⁵R. Bonifacio and L. A. Lugiato, Lett. Nuovo Cimento 21, 510 (1978).
⁶K. Ikeda *et al.*, Phys. Rev. Lett. 45, 709 (1980), and

48, 617 (1982).

- ⁷H. M. Gibbs *et al.*, Phys. Rev. Lett. 46, 474 (1981).
⁸W. Culshaw and J. Kannelaud, Phys. Rev. 136, 1209 (1964), and 141, 237 (1966).
⁹W. M. Doyle and M. B. White, Phys. Rev. Lett. 17, 467 (1966).
¹⁰W. Van Haeringen, Phys. Rev. 158, 256 (1967).
¹¹A. S. Lipatov and V. N. Parygin, Kvan. Elektron. (Moscow) 2, 2571 (1975), and 5, 2098 (1978) [Sov. J. Quantum Electron. 5, 1400 (1976), and 8, 1184 (1978)].
¹²A. Le Floch and R. Le Naour, Phys. Rev. A 4, 290 (1971).
¹³H. Haken, *Synergetics* (Springer, Berlin, 1978).
¹⁴We thank Dr. H. Thomas for calling our attention to the spatially competing order parameters in structural phase transitions; see K. A. Muller *et al.*, Phys. Rev. Lett. 25, 734 (1970).
¹⁵V. De Giorgio and M. O. Scully, Phys. Rev. A 2, 1170 (1970).
¹⁶W. W. Chow *et al.*, Opt. Commun. 15, 6 (1975).
¹⁷J. F. Scott *et al.*, Opt. Commun. 15, 13 (1975).
¹⁸P. Lett *et al.*, Phys. Rev. Lett. 47, 1892 (1981).
¹⁹M. Sargent, III, M. O. Scully, and W. E. Lamb, *Laser Physics* (Addison-Wesley, Reading, Mass., 1974).
²⁰L. Landau and I. Lifshitz, *Statistical Physics* (Pergamon, New York, 1958), Chap. 14.
²¹R. Bonifacio and L. A. Lugiato, Phys. Rev. Lett. 40, 1023 (1978).

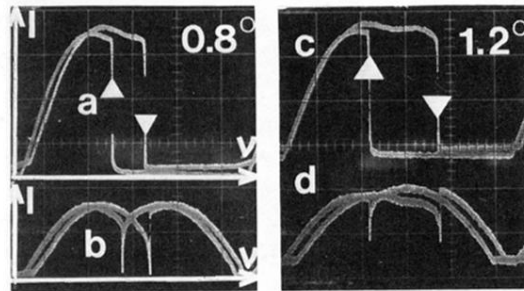


FIG. 2. The rotation mechanism. (a) Output power I of the x eigenstate polarization vs frequency for $\Delta\phi_{xy}=0.8^\circ$ (I axis, $3 \mu\text{W}/\text{div}$; ν axis, $60 \text{ MHz}/\text{div}$). (b) I with polarizer rotated at $\theta=\pi/4$ for $\Delta\phi_{xy}=0.8^\circ$. (c) Same as (a) for $\Delta\phi_{xy}=1.2^\circ$. Same as (b) for $\Delta\phi_{xy}=1.2^\circ$.

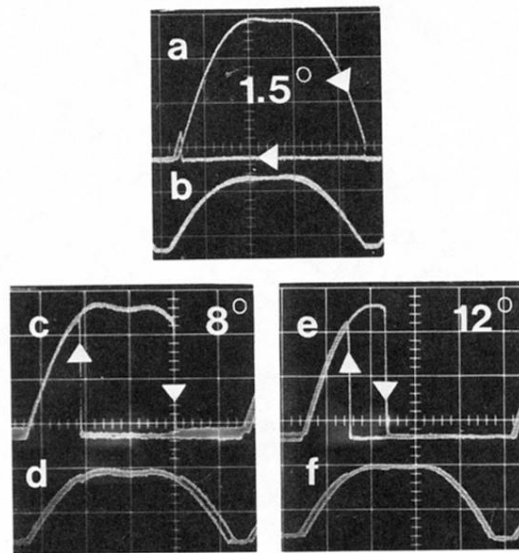


FIG. 3. The inhibition mechanism. (a) Same as in Fig. 2(a) for $\Delta\phi_{xy} = 1.5^\circ$. (b) Same as in Fig. 2(b) for $\Delta\phi_{xy} = 1.5^\circ$. (c) Same as (a) for $\Delta\phi_{xy} = 8^\circ$. (d) Same as (b) for $\Delta\phi_{xy} = 8^\circ$. (e) Same as (a) for $\Delta\phi_{xy} = 12^\circ$. (f) Same as (b) for $\Delta\phi_{xy} = 12^\circ$.

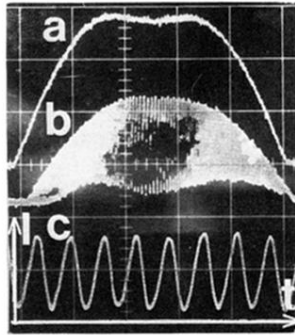


FIG. 4. Vectorial instabilities for $\Delta\phi_{xy} \approx 0^\circ$. Output power (a) vs frequency without polarizer, (b) vs frequency with polarizer, and (c) vs time at fixed frequency ($10 \mu\text{s}/\text{div}$).